3D Lacunarity in Multifractal Analysis of Breast Tumor Lesions in Dynamic Contrast-Enhanced Magnetic Resonance Imaging

Filipe Soares, Filipe Janela, Manuela Pereira, João Seabra and Mário M. Freire, *Member, IEEE*

***Abstract*—Dynamic contrast-enhanced magnetic resonance of the breast is especially robust for the diagnosis of cancer in high-risk women due to its high sensitivity. However, its specificity may be compromised since several benign masses take up contrast agent as malignant lesions do. In this article, we propose a novel method of 3D multifractal analysis to characterize the spatial complexity (spatial arrangement of texture) of breast tumors at multiple scales. Self-similar proprieties are extracted from the estimation of the multifractal scaling exponent for each clinical case, using lacunarity as the multifractal measure. These proprieties include several descriptors of the multifractal spectra reflecting the morphology and internal spatial structure of the enhanced lesions relatively to normal tissue. The results suggest that the combined multifractal characteristics can be effective to distinguish benign and malignant findings, judged by the performance of the support vector machine (SVM) classification method evaluated by receiver operating characteristics (ROC) with an area under the curve of 0.96. Moreover, the study confirms the presence of multifractality in DCE-MR volumes of the breast, whereby multiple degrees of self-similarity prevail at multiple scales. The proposed feature extraction and classification method has the potential to complement the interpretation of the radiologists and supply a computer-aided diagnosis (CADx) system.**

***Index Terms*—Breast Cancer, Classification, Computer-aided diagnosis, Dynamic contrast-enhanced, Feature extraction, Magnetic resonance, Multifractal analysis, Texture analysis.**

I. Introduction

MAGNETIC Resonance Imaging (MRI) of the breast has been shown to be the most sensitive modality for imaging high-risk women, offering valuable information about breast conditions that cannot be obtained by other imaging modalities, such as mammography or ultrasound [1], [2]. Dynamic contrast-enhanced magnetic resonance imaging (DCE-MRI) techniques are based on the injection of an MR contrast agent and acquisition of T1-weighted images over time, which provides information on the rate of passage of the agent between the blood and tissues. Tumor lesions are more vascularized due to angiogenesis than the surrounding normal tissue, and therefore these areas are distinguished from the background [3].

The diagnosis is generated by visual examination of morphology features and contrast-enhancement kinetics (functional features) using descriptors established in the Breast Imaging - Reporting and Data System (BI-RADS) lexicon [4]. Malignant lesions tend to have more irregular shape, spiculated margins, and heterogeneous inner enhancement [5]. A lesion with kinetics of rapid initial rise, followed by a drop-off with time (washout) in the delayed phase, can have a positive predictive value of 77% for malignancy [6], [7]. Although BI-RADS provides useful criteria, the priority and weights on different morphological features are not standardized. In addition, the analysis of functional features by radiologists is a time consuming task and a bottleneck in diagnostic workflow [8]. Fischer et al. [9] proposed the combination of DCE-MRI morphological and functional features for a scoring system (Göttingen score) that is nowadays useful to assess the BI-RADS grade. The reported values of sensitivity are frequently higher in DCE-MRI than any other breast imaging modality, whereas the specificity has been reported to fluctuate [10]. Indeed, clinical evaluation of breast MRI still remains largely subjective and the reported findings are often qualitative, having therefore an impact on the consistency and reproducibility of the interpretation [11]. Computer assisted interpretation arises in this context as an approach to reduce the subjectivity in human interpretation by improving specificity and possibly sensitivity, through an objective measurement, and offering the possibility of a reduction of the time needed for the breast MRI analysis [12].

To automate lesion classification, features extracted by computer-based image analysis have been investigated as diagnostic aids, with mathematical descriptors related with the ones visually used by radiologists [13]. This approach can be developed towards the quantitative analysis of textural, morphological and kinetic enhancement features.

Manuscript received August 28, 2012; revised January 26 and June 1, 2013. This work was partially funded by the Fundação para a Ciência e a Tecnologia through the grant SFRH/BDE/15624/2006, by Siemens S.A. Healthcare Sector, by Instituto de Telecomunicações and by University of Beira Interior, Portugal. *Asterisk indicates corresponding author.*

*Filipe Soares is with Siemens S.A. Healthcare Sector, 4456-901 Perafita, Portugal (e-mail: filipe.soares@siemens.com).

Filipe Janela and João Seabra are with Siemens S.A. Healthcare Sector, 4456-901 Perafita, Portugal.

Filipe Soares, Manuela Pereira and Mário M. Freire are with Instituto de Telecomunicações, Department of Computer Science, University of Beira Interior, 6201-001 Covilhã, Portugal.

Considerable efforts have been put on the development of computer-aided diagnosis (CADx) systems that give an impression about the suspicion level of the lesion. The general approach is based on tumor characterization and the application of automatic or semi-automatic classification. The simplest heuristic model used to distinguish between malignant and benign lesions in DCE-MRI is known as the three-time-points (3TP), [3], [14], where points are selected along the time-intensity sequence during contrast uptake to characterize the enhancement slope and the washout rate. The enhancement patterns in the 3TP method varies depending on imaging protocol, but all of the first post contrast series of malignant tumors with wash-out behavior in late phase do not show the peak contrast enhancement. Nevertheless, a plethora of other algorithms and classifiers have been proposed. The automated interpretation approach based on enhancement variance dynamics proposed by Chen et al. [15] used linear discriminant analysis for lesion classification after feature extraction. Later in [16], Chen et al. used the fuzzy c-means clustering technique to identify kinetics. For quantitative morphology analysis, Gilhuijs et al. [17] employed radial gradient histogram and other shape measures. Yao et al. proposed in [18] a pixel-by-pixel classification method based on texture analysis and wavelet transform for tumor evaluation in breast DCE-MRI. In [19], Zheng et al. used spatiotemporal enhancement pattern and Fourier transform to analyze two-dimensional images of breast tumors. Back-propagation neural network classification of segmented tumor regions was proposed by Meinel et al. [20] using a combined set of shape and kinetic features. The method for classification proposed by Nattkemper et al. [21] also includes both kinetic and morphological features and compares several classifiers of both unsupervised and supervised learning. Artificial neural networks have been one of the most investigated approaches for the classification of breast lesions in DCE-MRI [22-25]. However, it has been shown that support vector machine (SVM) lead to a better performance than a variety of other machine learning techniques when applied in discrimination of breast lesions [21], [26], [27].

Diagnostic findings in MR images of the breast may be disguised with respect to the surrounding features [28], since, for instance, non-mass vascular structures can dynamically enhance as malignant masses. In addition, some of the aforementioned studies that use classifiers of breast lesions in DCE-MRI apply a region analysis based on thresholding the enhancement signal [29], [30]. Once the signal intensity depends on the particular MRI instrumentation and contrast agent used in data acquisition, even fitting a pharmacokinetic model to the rise of intensities after contrast injection, there is no general approach for selecting threshold values. These methods require careful user interaction [31], hence other model-free approaches may be more suitable for classification of lesions with therapeutic changes of tissue perfusion and microvascular permeability.

Currently, the only fully-automated classification with reported use in the clinical practice is the one available in the first MRI CADx system DynaCAD® which solely relies on morphological analysis. The research behind this system is based on fractal theory as described by Penn et al. in [32], and focused on assessing the margin sharpness of the breast lesions, which is only one of the possible ways to analyze tissues in the breast [15], [17], [30], [33]. Moreover, a CADx system should also work as a second-look for the radiologist and therefore focus on a comprehensive set of characteristics of the lesions, including features that are indistinguishable to the human eye.

The fractal theory and the human tissue are related since both can be characterized by a high degree of self-similarity. In this context, self-similarity refers to images that have several parts looking like the whole image. When self-similar objects are evaluated, the irregularities are then considered as structural deviations from the global regularity of the background [34], [35]. In [36], Penn et al. have shown that nearly two thirds of the cancers were categorized inconclusive in terms of fractal dimension. A potential problem with the fractal dimension approach is that distinct fractal sets may share the same fractal dimension values with different appearances or texture patterns [37]. Therefore, the concept of lacunarity was introduced as a scale-dependent measure that describes the texture of a spatial pattern as a counterpart measurement of fractal dimension. Lacunarity explicitly characterize the spatial organization of an image, and its composing sub-units, which are potentially useful in representing the tumor inner structure. From the anatomical point of view, the lacunarity helps to estimate the spatial heterogeneity of the lesions when the object complexity given by fractal dimension is not enough. Guo et al. [38] explored the use of fractal and lacunarity analysis independently for the characterization of the spatial distribution of the pixel intensities and classification of mammographic images. Lacunarity was an effective counterpart measure of texture analysis. Both fractal and lacunarity studies rely on a measure as a function of scale. However, multifractal theory introduces a more advanced approach that allows a deeper exploration of the potential of the theory for medical image analysis. The multifractal analysis provides a spectrum of fractal dimensions, characterizing multiple irregularities. This can potentially provide more information about the image compared to the single fractal dimension [39], without being exclusively focused on lesion margins as in [36]. To the best of our knowledge, there are no further conclusive results of multifractal-based analysis in DCE-MR images of the breast. The closest work uses the Multifractal Detrended Fluctuation Analysis (MF-DFA) method [34] applied only in 2D Mammography, based on the structure of fluctuations and detrending steps without employing the lacunarity dimension. In this paper, we show how multifractal analysis may depend on the concept of lacunarity, when used for the description of the spatial distribution of the pixel intensities in image volumes with multiscaling behaviors.

Some studies have also been designed with the extraction of features in tri-dimensional (3D) volumes of interest (VOI). The performance is likely to improve when taking full advantage of the 3D nature of the MR data. In [17], a 3D

analysis was compared to two-dimensional (2D) analysis using a representative slice through the middle of the lesion. 3D was found to result in higher performance for the majority of the shape-based features. However, the manual lesion segmentation employed there would limit the inclusion of this technique in an automated CAD. Automatic segmentation has been shown to be useful when evaluating state-of-art features in 2D or 3D [40]. This is mainly due to the fact that these features rely on lesion morphology, and segmentation reduces the influence of normal tissue of the breast surrounding a tumor on that features. On the other side, usually the surroundings (background) of the lesions are not included in the analysis of texture complexity. The possible inner inhomogeneity of a mass and its relation to normal background is frequently ignored. Besides, most of 3D segmentation algorithms demand the use of connected-component labeling post-processing to remove scattered voxels not connecting to the main lesion [41]. This can lead to the modification of the original shape of the segmented tumor and classification errors. Moreover, sharp changes of the patterns of enhancement on border slices of a segmented tumor are known to occur with most of the techniques based on slice by slice assessment of the morphology. This results in lower specificity, probably caused by partial volume or the recently studied morphological blooming effect [32]. Blooming evaluates the transition of the margin to the surroundings by a progradient unsharpness of lesion borders, however, the spatial volumetric dependency was not investigated and multifractal approach has been also neglected as in [8]. Multifractal methods have the advantage of exploiting the differences in self-similarity properties between lesion and surrounding background. We therefore hypothesized that, in the task of distinguishing between malignant and benign breast lesions on DCE-MRI, multifractal texture analysis with lacunarity, as the multifractal measure, based on 3D isotropic volumes would yield improved performance than single or multi-slice 2D methods, whereas avoiding 3D segmentation and other post-processing.

In this article, we investigate the use of multifractal theory conditioned by the 3D lacunarity measure, for classification of breast lesions in DCE-MR volumes. We aim to evaluate new features for classification which characterize in more detail the morphology and texture of the contrast-enhanced breast lesions. This aim is accomplished by automated extraction of features from the multifractal scaling exponent and SVM-based classification of malignant and benign lesions. In order to study the irregularity patterns within a tumor relatively to its surroundings, the volumes selected include the normal background around the main lesion. The results obtained with the proposed method are compared within the same experimental setup with the MF-DFA 2D method, also based on multifractal characteristics, and with the 3TP, which represents a clinical standard for analysis of tumor kinetics.

II. Background and Theory

This section describes the theoretical background required to comprehend the proposed method specified in section III.

A. Multifractal analysis

Fractal dimensions are estimates of object complexity. They were originally developed to characterize geometrical patterns resulting from abstract recursive procedures called fractal processes [37]. Although fractal dimensions were developed for application to abstract mathematical objects, they can be applied to objects that do not arise from fractal processes, such as MR images [42], [43].

Fractals are self-similar in the sense that they have the same scaling properties, characterized by only one singularity exponent throughout the entire process. This means that when a part of a structure is removed and compared with the whole, they match. Self-similarity is a demanding model with respect to empirical data as it requires that scaling property holds for all scales and that a single Hurst (*H*) parameter controls all the statistical properties of the data. This is often a too severe limitation for practical purposes and multifractal models are preferred instead, which are considered as further extension to scale invariance since they enable to account for a declination of scaling properties often observed on empirical data. Moreover**,** in the same process we may notice similarity at different scales, located in different areas. This means that multiple fractal sets lie interwoven, each one with their own scaling behavior. Therefore, multifractals require a larger, and theoretically infinite, number of indices to characterize their scaling properties. Scaling refers to the propagation of energy or intensity when for example image data is inspected at various resolutions.

A multifractal object or process can be characterized through its spectrum by assessing which and how many fractal sets are associated to a certain influence (self-similarity trend) on time or space scale. These measures are provided with the dependence of the Hausdorff dimension *D(h)* from the Hölder exponent *h*, where *D(h)* represents the size of a certain trend with impact described by *h*. This multifractal spectrum describes the quality and quantity of irregularities in the data and its characteristic shape depends on periodic patterns [44].

A detailed description of the multifractal theory is beyond the scope of this article, but the reader is referred to e.g., [42], [44]. We only restate here a few key points. Multifractal analysis is based on the definition of a finite measure μ that can be considered as a mass distribution on a bounded subset of real numbers $\mathbb{R}^E$, where E stands for the Euclidean dimension of the space (E = 1, 2 or 3). For example, the distribution of a handful of sand on a box in a given point corresponds to the μ, a way to assign a numerical size to sets, such that if a set is decomposed into a countable pieces, then the size of the whole is the sum of the pieces sizes. This measure related with scale can estimate the local irregularity within that subset intersecting each cell of a linear grid map of size ε, i.e., for a multifractal measure μ, the partition function X has a power law relation with scale $r\varepsilon$ for variable range of moment order q, given by [45]:

$$X_q(r\varepsilon) \propto r\varepsilon^{\tau(q)}. \quad (1)$$

For simplicity, the parameter q can be seen as the focus control of a photographic lens for exploring different regions of irregularity. For $q > 1$, $\tau(q)$ represents the more singular regions, for $q < 1$, it accentuates the less singular regions and for $q = 1$, it represents the information dimension. The scaling exponent $\tau(q)$ has a concave shape that hence departs from the linear behavior qH, known as the signature of self-similarity. $\tau(q)$ can be seen as a collection of scaling exponents replacing the single self-similarity parameter H and, hence, conveying versatility in actual data analysis [46]. Multifractal analysis is often theoretically phrased in terms of multifractal spectrum $D(h)$ rather than $\tau(q)$, even though both function are related by a Legendre transform [37]. It also requires the measurement of q, a range that should be carefully chosen according to the data in study to avoid unstable power laws.

B. Lacunarity estimation

Lacunarity measures the deviation of a geometric object, such as a fractal, from translational invariance. It is a scale-dependent measure of heterogeneity that allows to distinguish between two fractals with the same fractal dimension. Lacunarity complements the fractal dimension that measures how much space is filled, by measuring how the data fills the space [45], [47], [48].

Lacunarity can be defined in terms of the local first and second moments (i.e., local mean and variance) measured for different neighbourhood sizes about every pixel within the image. Lacunarity as a function of neighbourhood size is generally presented as a double log plot, which illustrates the scale dependency of spatial nonstationarity in the image. Higher lacunarity values indicate more translational invariance, i.e., a wider range of sizes of structures within an image. The decay pattern of the lacunarity plot contains significant information about the spatial structure of the image. For example, a linear decay represents a self-similar fractal with no change in spatial pattern or texture with window size [49].

Based on the analysis of the mass distribution in a deterministic or a random set, Allain and Cloitre [50] proposed a gliding box algorithm for lacunarity estimation. This method involves the assessment of the variance of the box mass M at each step, where the mass is the sum of white pixels in a gliding box along the coordinates in the Euclidean space. This procedure is repeated as the box moves pixel by pixel through the whole region. The probability distribution, $Q(M, r)$, is then calculated as the ratio of the number of gliding boxes with the lateral size r and mass M over the total number of boxes. The lacunarity at scale r is then defined by the mean-square deviation of the fluctuations of mass distribution probability $Q(M, r)$, divided by its square mean [50], as follows:

$$\Lambda(r) = \frac{\sum_{M} M^2 Q(M,r)}{\left[\sum_{M} MQ(M,r)\right]^2}, \qquad (2)$$

where M can be calculated according to the purpose of application and problem requirements, since lacunarity estimation is not confined to binary configurations but can also be used with grayscale images [51], [52].

III. 3D Multifractal Scaling Exponent Lacunarity Analysis (MF-SELA)

In this section, the method proposed to characterize the tri-dimensional complexity, or spatial arrangement of texture roughness of breast tumors, is described.

Through the theory it is stated that the dynamics of scaling can be used as discriminatory descriptors, providing an additional perspective of the data when inspected at various resolutions. Furthermore, in this study it was attempted to confirm that selected VOIs from breast MRI have multiple degrees of scaling by the prevalence of a multifractal spectrum $D(h)$ or a non-linear multifractal scaling exponent $\tau(q)$.

Fig. 1 illustrates the flowchart of the model for the decision-support in the diagnosis of breast cancer with DCE-MRI. The cases and respective clinical reports are the input of the model. The analysis scheme proceeds to the pre-processing and selection of a grayscale VOI in which the multiscale extraction of features related with self-similarity, the core of the model, takes place. Herein the framework of the implementation is a gliding cube, which is an extension from the efficient estimation of the gliding box lacunarity presented in [47]. The features are extracted from the estimation of the scaling exponent, taking advantage of using 3D lacunarity as the measure to feed the multifractal characterization of the VOI, which includes the lesion and surroundings, at multiple scales.

In addition, it is worth notice that in the present work the pixel intensity is not considered as extra dimension, as in [53], [54]. Dong et al. [48] shown that spatial patterns of 3D points, not images, with different degrees of heterogeneity can be separated using lacunarity, and those that cannot be discriminated from each other at one scale can be separated at some other scales. Also distinct is the work in [55], since a multifractal modeling used to validate an experimental method of lacunarity estimation should not be confused with the multifractal analysis of images proposed here. Our estimation of a scale-dependent degree of heterogeneity given by the lacunarity emerges as the multifractal measure of complexity that will allow the multiscale extraction of features, namely texture and its distribution in each DCE-MRI case.

The entire procedure of the 3D Multifractal Scaling Exponent Lacunarity Analysis (MF-SELA) includes four major steps: (A) Pre-processing and VOI selection, (B) 3D lacunarity estimation with gliding cube, (C) Multifractal analysis with 3D lacunarity, (D) Self-similarity and scaling dynamics as descriptors.

A. Pre-processing and VOI selection

Voxels are usually anisotropic in breast DCE-MRI, i.e., the spatial resolution in the cross-slice direction is poorer than in plane. Thus, a bi-linear interpolation was used to yield isotropic voxels in the volume image. This pre-processing step

is a requirement for the multifractal method proposed, as described below.

A cubic VOI of lateral size between 32 and 64 pixels was cropped from each 3D MRI, according to the location and size of the lesion defined in the BIRADS report by the radiologists. This was performed in a subtraction image, of the first post-contrast acquisition after contrast arrival subtracted from the pre-contrast image. In order to study the inherent properties of the lesions relatively to its surroundings, the VOI includes not only the lesion but also the normal tissue. The effect of the amount of non-lesion background on multifractal analysis was assessed by selecting variable VOI sizes centered in the same lesion point. This coordinates are inputted manually and the remaining stages are fully automated.

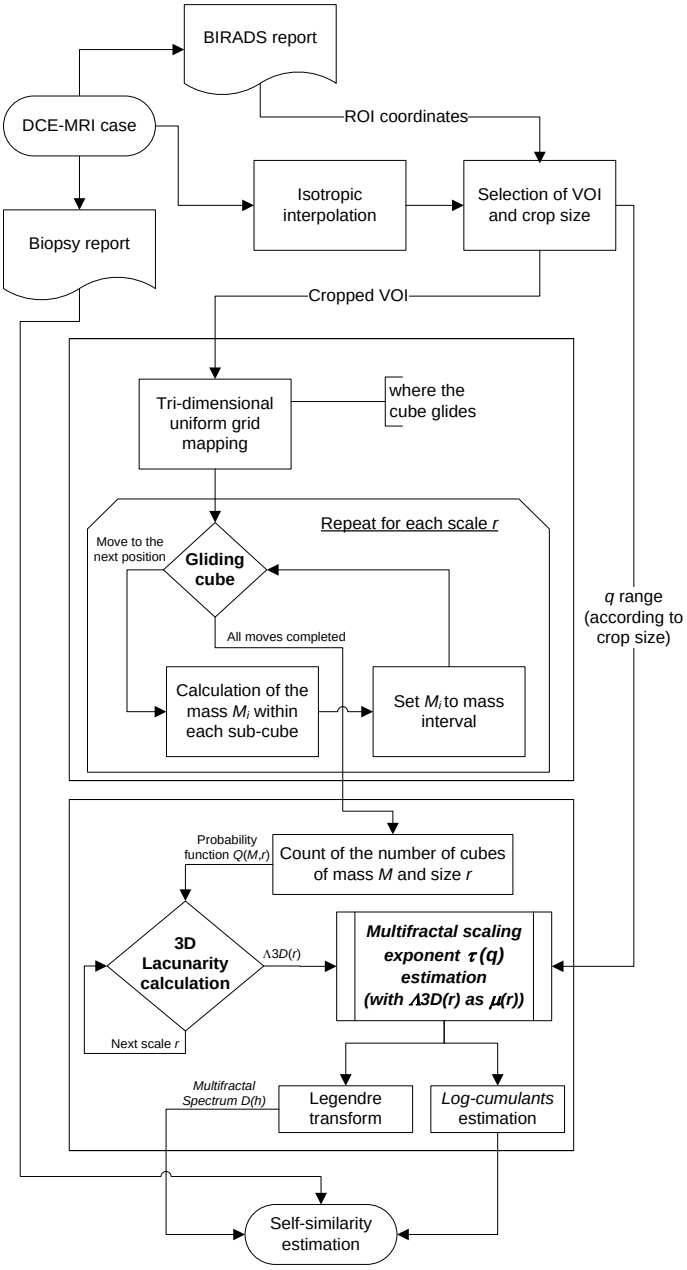

Fig. 1. Flowchart of the model for Multifractal Scaling Exponent Lacunarity Analysis (MF-SELA).

B. 3D lacunarity estimation with gliding cube

As a base level, we start by mapping a 3D uniform grid where the cube glides. Based on (2) and using accumulated statistical moments as the cube glides through the VOI [47], the gliding cube estimation of lacunarity is proposed herein by

$$\Lambda 3D(r) = \frac{N(r)\sum_{i=1}^{N(r)} M_i{}^2 n(M_i, r)}{\left[\sum_{i=1}^{N(r)} M_i n(M_i, r)\right]^2}, \quad (3)$$

where for each gliding along every grid position, the mass M within the ith cube is carried as well as the running sums needed to calculate $n(M, r)$, here extended to number of cubes with mass M and lateral size r, being $N(r)$ the total number of cubes of size r. This required a partition of mass intervals for counting purposes and, therefore, an extra parameter of interval precision in our proposed method of lacunarity analysis. M was calculated for each cube by adding the grayscale intensity values of the voxels contained in the cube divided by the cube volume. This approach revealed better discrimination power in the last steps of the MF-SELA, with our validation experiments, when compared with other alternatives like the relative intensities used in [54], [55]. The reason why isotropic voxels were required and the images were interpolated is due to the usage of a cubic neighborhood, that constrains the expression of the spatial heterogeneity to translational invariance, in a similar way to [56], [57] for self-similarity estimation.

As r increases with respect to the base level grid, the procedure raises its efficiency while the number of gliding cubes tends to one and the $\Lambda 3D(r)$ measure tends to zero. Since we are not working with exactly pure self-similar fractals, it is important to calibrate the range of scales according to the empirical data. This problem was already raised in Section II.A concerning multifractal analysis. Too small or too large limits of r can cause disturbance of linearity in the lacunarity function, as it is common with fractals [58]. Therefore, after calibration with DCE-MRI data, the MF-SELA was parameterized with r ranged from 6 to VOI size/4. Finally, the complexity of the fundamental operation of 3D lacunarity estimation is $O(n^3)$, where n is the dimension of the interpolated VOI.

C. Multifractal analysis with 3D lacunarity

Multifractal analysis exploits both the local irregularity (often seen as texture roughness or complexity) of a given object and the global distribution of this irregularity, as reported in [34]. The next step of MF-SELA is the core multifractal analysis of the VOI, to obtain the scaling exponent and multifractal spectrum.

Fractal and multifractal analysis often involves partitioning the space of study into subsets to build samples with multiple scales. The number of the samples at a given scale is limited by the size of the partitioning space and data resolution (sampling resolution), which is usually the main factor influencing statistical estimation. Several techniques have

been developed for estimating multifractal *D(h)* by means of the box-counting algorithm [39]. Gliding box methods can be integrated into the existing multifractal techniques such as the moment method. Here the multifractal analysis begins with the estimation of $\tau(q)$ that controls how the moments of measure μ scale with r. Cheng et al. [59] proposed a gliding box alternative for implementing the moment method in multifractal analysis as follows:

$$\langle \tau(q) \rangle + E = \lim_{r \to 0} \frac{\log\left(\frac{1}{N(r)}\right) \sum_{i=1}^{N(r)} \mu_i{}^q(r)}{\log r}, \quad (4)$$

where $\langle\rangle$ stands for statistical moment with measure $\mu \neq 0$. This method was generalized for 3D in our implementation. Consequently, it is possible to obtain larger sampling resolution, precisely one of the common drawbacks of DCE-MR volumes, leading to better statistical results [59].

The measure μ in the scope of MF-SELA is defined as the mass distribution given by $\Lambda 3D(r)$ as

$$\sum_{i=1}^{N(r)} \mu_i{}^q(r) \equiv \Lambda 3D^q(r). \quad (5)$$

Accordingly, by using (4) and (5) it is possible to obtain the scaling exponent $\tau(q)$ that can later be used for estimating the multifractal spectrum *D(h)* as explained in Section II.A. This approach of a scaling exponent with a gliding box estimation of 3D lacunarity end-up being the key point for multifractal characterization of a VOI, by

$$\langle \tau(q) \rangle + E = \lim_{r \to 0} \frac{\log\left(\frac{1}{N(r)}\right) \Lambda 3D^q(r)}{\log r}. \quad (6)$$

D. Self-similarity and scaling dynamics as descriptors

The existence of a distribution or spectrum *D(h)* may confirm the presence of multifractality, as multiple degrees of self-similarity can be estimated at multiple scales. Given $\tau(q)$ and *D(h)* outcome of multifractal analysis of a VOI, the last step of MF-SELA is the extraction of features related with the spatial arrangement of voxel intensities (texture) in the images of breast tumors. This can be achieved by studying the dynamics of the scaling as multifractal descriptors that may be linked with morphology and internal spatial structure of the enhanced lesions to discriminate.

Different spectral characteristics are quantified from *D(h)*, that is directly related with the irregularity of the analyzed object. The higher *D(h)*, the more frequently we can find intensity changes of a specific type *h*. One important descriptor studied is precisely the *h* where the spectrum is maximum. It shows at which Hölder exponents is positioned the most statistically significant part of the VOI, i.e. the subsets with maximum fractal dimension. Hurst parameter (*H*) is often associated with this exponent reminding the monofractal theory where there is only one fractal dimension. Curve width (*W*) can be a descriptor related to how far from monofractal a ROI is. Multifractal analysis focuses on exploring and understanding the nature of the irregularities in the image, and not on a single, most prevalent irregularity, or global trend. Other important descriptors can be right slope (*RS*) of the curve, from the rightmost Hölder point ($R\alpha$) to the maximum *D(h)*. On the other side, *LS* represents the slope of the distribution of the collection of Hölder exponents below *H*, where large fluctuations from the global irregularity (most prevalent) are exploited.

A unique parameter that combines the previous ones has been introduced to better differentiate the MR cases. This suggestion of a single parameter was introduced by [60], with a distinct use of descriptors and with application in brain imaging. The combined spectral parameter (*CP*) proposed in this work for multifractal analysis of DCE-MRI of the breast, is determined as a ratio between *H* and *LS*. This specific combination leads to low values for simple random noise intensities of the VOI, and result in high *CP* for VOIs containing more complex properties due to tumor presence in self-similar background. Hence, we raise the hypothesis that *CP* can be a reasonable measure for distinguishing likelihood of malignancy of breast cancers.

Moreover, an empirical scaling analysis of the multifractal scaling exponent $\tau(q)$ has been suggested to be studied as a polynomial expansion of order *p* [61]

$$\tau(q) = \sum_{p \geq 1} c_p \frac{q^p}{p!}, \quad (7)$$

instead of measuring $\tau(q)$ by estimation for all *q*. The *log-cumulants* c_p can be obtained from the scale dependence of *C(j,p)*, the cumulant of order $p \geq 1$ and scale *j*, of a random variable *X*. Equation (7) implies that *C(j,p)* must satisfy [62]

$$C(j, p) = c_p^0 + c_p \ln 2^j. \quad (8)$$

Therefore, the study of $\tau(q)$ and hence *D(h)* can be rephrased in terms of the log-cumulants. This is interesting since a process is said to be multifractal when $\tau(q)$ departs from linear behavior with $c_2 \neq 0$. The most practically used *Log-normal* multifractal can be characterized only by c_1 and $c_2 \neq 0$, but more complex multifractal models may involve polynomials of higher order than 2. The log-cumulants can be estimated by linear regression, with c_1 being related with the location of the *H*, while c_2 with its width, and c_3 possibly characterizing the asymmetry of *D(h)*.

This article aims to evaluate if the VOIs from the DCE-MRI of the breast can be represented or not by $p \geq 2$, $c_p \neq 0$ and thus reveal a simple or more complex multifractal behavior, by rephrasing $\tau(q)$ in terms of the log-cumulants estimated by linear regression as

$$\tau(q) = c_1 q + c_2 \frac{q^2}{2!} + c_3 \frac{q^3}{3!}. \quad (9)$$

We retain the characteristics that allow differentiating tumoral tissues from healthy tissues. The ranges of multifractal descriptors and log-cumulants which correspond to malignant areas will be set, and classifiers will be obtained.

IV. Experimental setup and performance assessment

The validation of the MF-SELA proposed was carried out using the following experimental setup. Here we provide details about how the images were acquired, what type of lesions were diagnosed by the radiologists and followed by a biopsy intervention resulting in a histological proof, as illustrated in the beginning of the flowchart in Fig. 1. The section ends with the description of a SVM-based supervised learning technique for classification of malignant and benign lesions.

A. Image acquisition

Experimental data was acquired using a Siemens Trio 3T MR Scanner at the health institution Clínica João Carlos Costa, Viana do Castelo, Portugal. Written informed consents were obtained from the patients as well as the approval from the institution's research ethics committee for this study. Dynamic imaging was performed using a T1-weighted FLASH 3D (FL3D) pulse sequence with fat saturation. The patients were scanned in prone position using a standard double breast coil. The acquisition protocol parameters were 3.76 ms of repetition time, 1.38 ms of echo time with flip angle = 12º. Each slice contains 448 × 448 pixels and has a typical field of view of 30 × 30 cm^2, yielding an in-plane spatial resolution of 0.65 × 0.65 mm^2 and a slice thickness of 0.6 mm for the generated 3D volumes. Imaging is performed before and after a bolus intravenous injection of 0.1 mmol/kg of Gadopentetate dimeglumine (Gd-DTPA). Five bilateral axial acquisition series were taken per patient at intervals of 1 min and 51 seconds. The first post-contrast images acquired after contrast arrival were used for the analysis of the enhanced lesions since it was found that the information from the initial portion of the time was the most predictive of malignancy as reported in [41] and [63].

B. Tumor collection and diagnosis

The initial database of 130 consecutive clinical cases was collected from August 2009 to May 2011 and retrospectively analyzed, not including vascular structures, architectural distortions and other non-masses. It is important to note that in this work "case" refers to a physical lesion, not a patient. Patients were previously checked for renal function as part of clinical routine for MR contrast administration. No pregnant women were included and patients with breast implants posed additional difficulties and they were excluded from the present analysis in breast DCE-MR. There was no exclusion criterion concerning the type of benign or malignant tumor.

A diagnosis report was processed by radiologists with a BI-RADS grade assigned for each case, depending on the morphology (see Fig. 2) and dynamic enhancement (Fig. 3) of each finding. A total of 35 lesions had biopsy recommendation and underwent to histological examinations. According to these pathology-proven cases, the clinical positive predictive value for biopsy was only 62% and, for that reason, these cases were included in our analysis. Consequently, the working dataset is composed of 15 malignant and 20 benign lesions. Table I shows the histopathology and disease state of the clinical cases analyzed. The most prevalent type of benign lesion was the fibroadenoma, being the invasive ductal carcinoma the most prevalent among the malignant histological proofs. The sizes of the lesions are evenly distributed among the malignancy (see Fig. 4). The longest diameter was estimated by radiologists using an electronic ruler, where the lesion was best visualized. Focus and foci are enhancements measuring less than 5 mm in diameter that are too small to be characterized in MR data and cannot be otherwise specified. These lesions are typically stable on follow-up, may result from hormonal changes and are considered to be a part of the normal background enhancement pattern in the breast [4], [6]. The final cohort of patients had an average age of 47 ± 9 years and an average weight of 66 ± 6 kg.

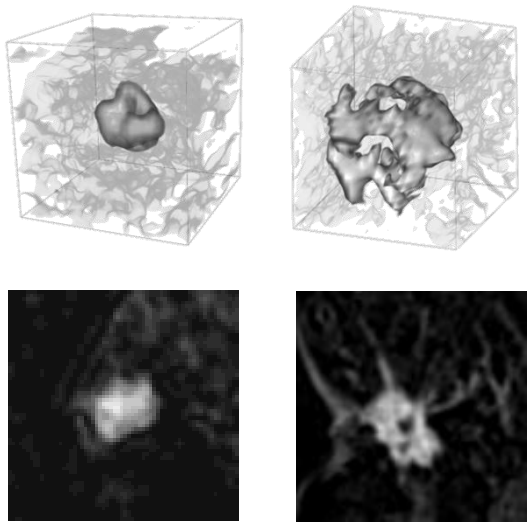

Fig. 2. Morphology features of lesions in the dataset. Representation of tumor VOIs (top). A sliced region of interest of a typical: benign case (bottom left), with oval shaped mass smooth, margin and homogeneous enhancement; malignant case (bottom right), with irregular shaped mass, spiculated margin and heterogeneous enhancement

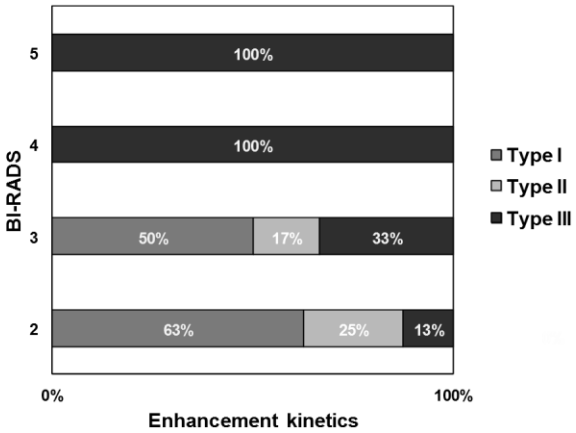

Fig. 3. BI-RADS grade of the lesions in the dataset plotted against the kinetic curve types of contrast enhancement as determined by radiologist.

TABLE I
CLINICAL CASES IN THE DATASET

Case ID	Patient ID	Longest dimension (cm)	BIRADS	Histopathology	Disease state
01	P01	2.5	5	IDC	Malignant
02	P02	2.8	3	Fibroadenoma	Benign
03	P03	1.9	4	Sclerosing Adenoma	Benign
04	P04	1.6	4	DCIS	Malignant
05	P05	1.8	3	Fibrocystic changes	Benign
06	P06	1.4	6	DCIS	Malignant
07	P07	2.8	2	Fibroadenoma	Benign
08	P08	1.7	3	PASH	Benign
09	P09	0.8	4	Myoepithelial cells	Benign
10	P10	6.8	6	IDC	Malignant
11	P11	4.2	4	PASH	Benign
12	P12	2.9	2	Fibrocystic changes	Benign
13	P13	0.5	4	IDC	Malignant
14	P14	3.8	6	IDC	Malignant
15	P15	1.4	6	DCIS	Malignant
16	P16	1	4	Fibroadenoma	Benign
17	P17	0.9	3	DCIS	Malignant
18	P18	2	4	Stromal fibrosis	Benign
19	P19	2.9	2	Fibroadenoma	Benign
20	P19	1.5	3	Lymph node	Malignant
21	P20	4.1	5	IDC	Malignant
22	P20	7.8	5	DCIS	Malignant
23	P21	1.3	4	LCIS	Malignant
24	P21	0.8	4	IDC	Malignant
25	P22	1	4	Fibroadenoma	Benign
26	P23	2.5	2	Fibroadenoma	Benign
27	P23	1.5	2	Fibroadenoma	Benign
28	P23	1.8	2	Fibroadenoma	Benign
29	P24	2.4	6	IDC	Malignant
30	P25	0.7	2	Fibroadenoma	Benign
31	P26	2.3	2	Fibrocystic changes	Benign
32	P26	1.3	4	Fibroadenoma	Benign
33	P26	1.8	4	DCIS	Malignant
34	P27	0.7	3	Fibrocystic changes	Benign
35	P27	0.6	4	Fibrocystic changes	Benign

Ductal Carcinoma In Situ (DCIS), Invasive Ductal Carcinoma (IDC), Lobular Carcinoma In Situ (LCIS), Pseudo-angiomatous Stromal Hyperplasia (PASH).

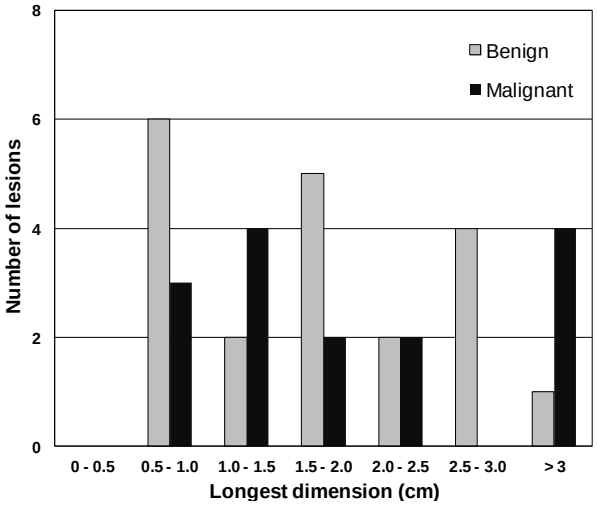

Fig. 4. Histogram of the longest diameter of the lesions in the dataset. The longest diameter was measured where the lesion was best visualized as determined by radiologist.

C. SVM-based classification

Classification of tumors as malignant or benign was performed by applying SVMs with the extracted multifractal-based features, each SVM using just a single feature. The role of multifractal descriptors and log-cumulants are still and open problem for the characterization of tumors. The single feature independent classification was adopted instead of using all features jointly to better understand ROC curve differences, among all of these features with distinct theoretical meaning. SVM-based classification was performed using the SVM^{light} [64] open source package for its efficient optimization algorithm, which allows choosing multiple kernel functions and its parameters to obtain a different classification hyperplane. Radial Basis Function (RBF) that requires the parameter gamma γ was the kernel used in this work. The condition for optimal hyperplane also includes a regularization parameter C that controls the trade-off between maximization of the margin and minimization of the training error. Small C tends to emphasize the margin while ignoring the outliers in the training data, while large C may tend to over fit the training data.

In order to determine which type of kernel function to use, its associated parameters, and C in the structural risk function, i.e. to select the possibly optimal model for our classification problem, we applied Leave-one-out (LOO) cross-validation to the working dataset [64]. This LOO technique involves training the machine learning algorithm for estimating the likelihood of malignancy from all cases but one, testing classification on that single case. This procedure is repeated until each case has been tested individually. The cross-validation ensures that all elements of the dataset are may be used for both training and testing. Misclassification errors were averaged to obtain an estimate of the generalization error of the SVM classifier. Our approach to yield the best classification based on each feature was to choose the parameters of SVM that produce the model with smaller errors in the cross-validation and use it for testing in order to maximize the accuracy.

D. ROC analysis

The capability of the features in distinguishing between malignant and benign lesions are further examined and evaluated by receiver operating characteristics (ROC). The area under the ROC curve (A_z) was used as a performance measure of the discrimination power of the individual features and of the SVM classification in a LOO scheme.

In order to more accurately place our method in the landscape of breast lesions classification, we applied a clinical standard protocol, the 3TP technique, to our dataset. On the other hand, we sought to evaluate the effect of skipping the lacunarity measure in the multifractal analysis to better understand the source of our performance. As lacunarity is intrinsically associated to the 3D analysis in the method proposed, we used a previously implemented 2D multifractal analysis (MF-DFA 2D) for comparison in the same setup, also evaluated with ROC analysis.

V. Results

The first major validation of the applicability of the methodology was achieved by verifying that the data possess multiple scaling properties. Fig. 5 shows the multifractal spectra of the analyzed VOIs where several degrees of scaling prevail for all the cases, as they are not limited to a single Hölder exponent. We can see that the *D(h)* curves are quite similar in shape and span. However, looking solely at the spectra the distinction between benign and malignant tumors remains unclear. In order characterize the multifractal spectra of the VOIs from the clinical cases studied, the aforementioned (see Section III.D) spectral descriptors were quantified. Another verification of the multifractality resulted from studying scaling exponent $\tau(q)$ (see Fig. 6) through the estimation of log-cumulants, as it may be confirmed in Fig. 7 that c_1 and $c_2 \neq 0$. The concavity of $\tau(q)$ in Fig. 6 implies non-normalized values of $c_2 < 0$.

All features investigated in this study show moderate potential for distinguishing between benign and malignant lesions, relating the measurements in Fig. 7 (top) directly with likelihood of malignancy. However, false negatives arise as represented by the outliers from the top in the benign boxes. Those report cases with a strong enhancement and all morphological characteristics of malignancy. In addition, false positives occur in-between zone of the box-plots from benign and malignant groups. This had reinforced the need for a better multifractal descriptor. A statistical analysis was further conducted by One-way analysis of variance (ANOVA) followed by a Post-Hoc Tukey test corrected for multiple comparisons (see Fig. 7, bottom). *CP* was proposed as several descriptors (with statistically significant differences) were combined and *H* (strongest irregularity) against *LS* (inner enhancement) resulted better than the others.

Fig. 8 and Table II present the performance of the proposed method evaluated by the area under the ROC curve for the SVM classifiers using each feature. Smoothed ROC curves were generated according to the binormal model [66]. The A_z of the discrimination was calculated varying a threshold level on each feature to separate benign and malignant groups. For all features analyzed, it is observed that SVM classification produced higher A_z values than the discrimination alone. The combined parameter *CP* and the individual *LS* and *RS* stand out as better features with higher A_z and lower testing error (TE) with SVM. The complementary shape of the ROC curves from *H* and *LS* justifies the maximum A_z obtained with *CP*. Statistically significant differences (p-value < 0.05) were found between A_z corrected for multiple pairwise comparisons (using MEDCALC): *CP* vs. *H*, *W*, *c1* and *c3*.

It is also worth noting that for the estimation of $\tau(q)$ several ranges of q were tested (results no shown), leading to an optimal discrimination power of lesions with $-4.3 < q < 2.1$ for the problem in study. The chosen q range includes interval steps adapted for the multiple sizes of VOI tested according to our DCE-MRI data to avoid unstable power laws and statistical errors leading to better ROC performance, without compromising the computational performance. The average execution time per case of the entire MF-SELA is 7.89s, on a 2.53-GHz Intel® Core™ i5 M540 workstation.

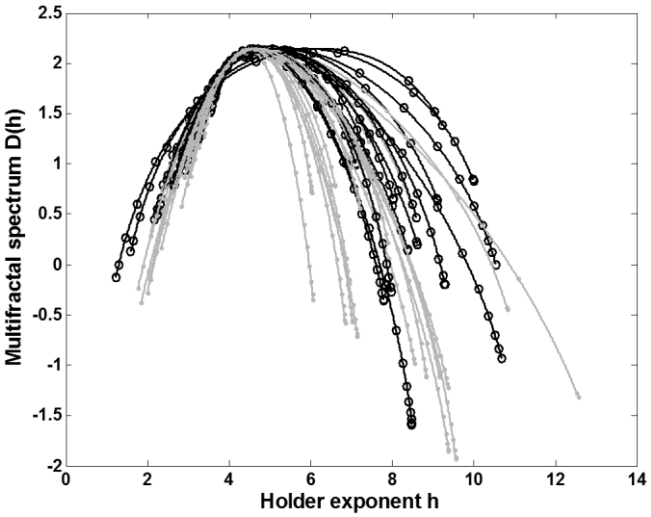

Fig. 5. Multifractal spectra *D(h)* of the VOIs of the cases in the dataset. Benign cases in gray. Malignant cases in black.

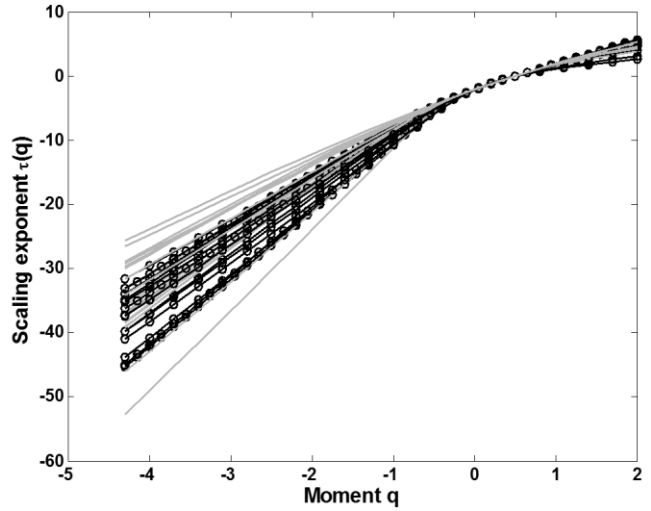

Fig. 6. Multifractal scaling exponent $\tau(q)$ of the VOIs of the cases in the dataset. Benign cases in gray. Malignant cases in black.

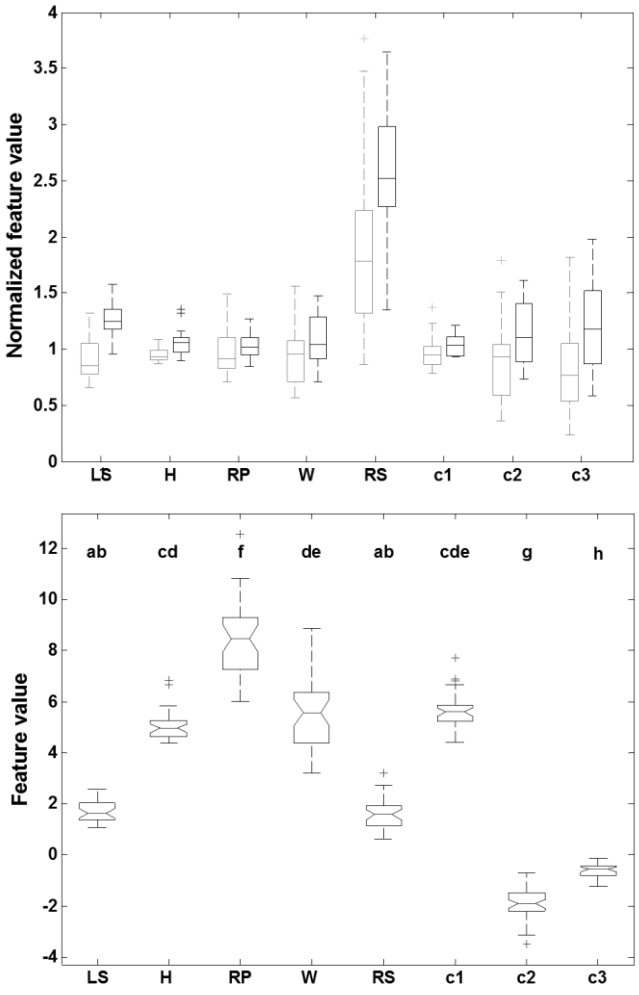

Fig. 7. Comparison of multifractal descriptors and log-cumulants as features. Top: For each feature normalized by its mean value, benign cases in gray and malignant cases in black. Bottom: Pooled features values tested for statistically significant differences with One-way ANOVA resulting in *F*-statistic = 588.32 and *p*-value < 0.05. Statistically significant differences among descriptors are identified by letters according to Post-Hoc Tukey test.

TABLE II
AREA UNDER THE ROC CURVE A_z IN DISCRIMINATING MALIGNANT FROM BENIGN LESIONS WITH MULTIFRACTAL-BASED FEATURES. A_z OF THE SVM CLASSIFIER USING EACH FEATURE (LEAVE-ONE-OUT CROSS-VALIDATION)

	Discrimination		SVM classification				
Feature	A_z	(± STD)	A_z	(± STD)	γ	C	TE
CP	0.868	0.050	0.960	0.027	6	10	0.1429
LS	0.896	0.050	0.901	0.055	6	10	0.2286
H	0.786	0.076	0.795	0.076	6	10	0.2286
RP	0.617	0.097	0.873	0.062	8	10	0.1714
W	0.643	0.091	0.760	0.081	6	100	0.2571
RS	0.726	0.091	0.898	0.063	6	1000	0.1714
c1	0.672	0.079	0.685	0.086	0.6	10	0.3143
c2	0.695	0.087	0.800	0.061	6	100	0.2286
c3	0.736	0.087	0.763	0.076	2	1000	0.2571

Gamma γ and regularization parameter (*C*) as associated kernel parameters and corresponding expected testing error (TE).

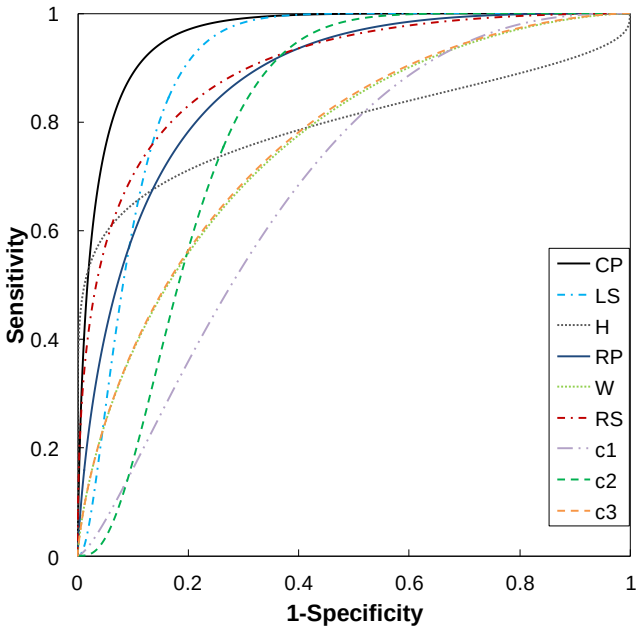

Fig. 8. ROC curves comparing the classification performance of the multifractal features and the combined parameter (*CP*) using SVM with a leave-one-out testing.

Table III presents the A_z obtained when applying three different methods to our dataset: 3TP, another multifractal approach MF-DFA 2D and MF-SELA 3D. The A_z obtained with the multifractal methods is well above the 3TP performance.

TABLE III
ROC A_z OF 3TP AND TWO MULTIFRACTAL METHODS ON OUR DATASET OF 35 CASES

Method	3TP	MF-DFA 2D	MF-SELA 3D
A_z	0.71	0.87	0.96

VI. DISCUSSION

DCE-MRI is useful in evaluating lesions that appear morphologically benign on conventional imaging studies. Diverging results were published concerning the diagnostic value of the lesion enhancement rate in the time course data [3]. Radiologists identify cancers with benign-like kinetics and normal tissues that exhibit cancer-like morphology. Therefore, we suggest that further features might be beneficial for the diagnosis of a breast cancer. In the early post-contrast period, it is established that the enhancement serves as a differential diagnostic criterion, with malignant lesions exhibiting stronger and faster enhancement than benign changes do [4]. In fact, this was verified in our preliminary experiments in [35] and confirmed in this work. We found that the information from the initial portion of the time was the most predictive of malignancy and, consequently, the first post-contrast images acquired after contrast arrival were used for the analysis of the enhanced lesions.

The proposed MF-SELA (see Fig. 1) establishes a multifractal analysis with a tri-dimensional lacunarity $\Lambda 3D(r)$ as measure to obtain the scaling exponent and multifractal

spectrum. $\Lambda 3D(r)$ is estimated using the gliding cube method, with the advantage of large sample size that usually leads to better statistical results. Self-similarity features of the $\tau(q)$ and $D(h)$, automatically generated for each early post-contrast volume image acquired after contrast arrival, were analyzed quantitatively. This quantification of features values should not be confused with the quantification of signal intensity values of voxels.

For our working dataset, the radiologists from the medical institution where the images were acquired reported 60% of specificity at 87% of sensitivity as diagnostic performance. Experimental results shown here by ROC curves reveal higher specificity at the same level of sensitivity with five features (*CP*, *LS*, *RS*, *RP* and log-cumulant c_2) derived from multifractal theory. SVM-based classification of the likelihood of malignancy of breast tumors showed good performance with VOIs containing mass lesions and their surroundings. Results suggest that *CP* and *LS* are the most appropriate feature for characterizing the inner texture heterogeneity of a VOI at different scales, with higher values for malignant cases. ROC analysis demonstrated that approximations of the $\tau(q)$ by the log-cumulants does not provide a complete characterization of the texture with sufficient discrimination power. However, the SVM classifier using the feature c_2 produced the best performance among the log-cumulants, with higher A_z than its theoretically related *W*. The main benefit of the log-cumulant triplet (c_1, c_2, c_3) was to emphasize the difference between $\tau(q)$ that departed from linear in *q*. This was confirmed in practice by approximating the function $\tau(q)$ with limited number of c_p that could simplify the classification task based on multifractal analysis.

For the computer-extracted features to be accepted, the link with morphology descriptors defined in BI-RADS lexicon needs to be established. Concerning lacunarity nothing should be discussed as its value was not directly used as a feature, but as a multifractal measure to compute the spectra $D(h)$. However, regarding self-similarity, it was found that H was related with the most prevalent irregularity in the VOI, namely shape and margins.

The descriptor *W* and log-cumulant c_2 are related to inhomogeneous degree of enhancement regularity (texture) and theoretically how far from monofractal a ROI is. *W* is generally bigger in malignant cases that represents richer scaling behavior compared to benign lesions. In addition, the more negative unnormalized value of c_2 the stronger the experimental evidence in favor of multifractality. Negative findings (no enhancement, results not shown) wherein there is nothing to comment on, *W* and c_2 tend to zero. False negative detection of findings can be depicted based on this criterion.

The descriptor Hurst parameter (*H*) shows at which Hölder exponents (*h*) is positioned the most statistically significant subsets of VOI voxels with maximum fractal dimension. This is directly related with the irregularity of the analyzed VOI, and it was slightly lower for the benign cases. Besides this prevalent scaling behavior, a multitude of other scalings might be present although occurring much less frequently.

Smaller slopes of *LS* reveal further scaling of large fluctuations from the *H*. Benign lesions with lower slopes show more sharp transitions of intensities that are different from the global irregularity. The *RS* descriptor represents the slope of the distribution of the collection of Holder exponents above *H*, where small fluctuations from the global irregularity could be analyzed. Thus, the higher *RS* of malignant cases can be seen as a weaker scaling pattern of the smooth variability relative to the most prevalent characteristic irregular *H*. On the other hand, for the associated scale parameters (*q* and *r*) chosen, the role of *RP* translates into the limit where it is possible to define a smooth variation from the global regularity. The bigger the limit for a case, the larger multi-scale heterogeneity is present.

In a general interpretation, the malignant cases are more globally inhomogeneous, show higher contrast-enhanced changes that are anti-persistent, and lower contrast-enhanced changes with persistence. However, the false-positives in each individual descriptor had lead to a new proposed descriptor (*CP*), which combines previous ones intending to improve the differentiation of the tumor cases.

In computer-aided diagnostics, it is very important to obtain a machine learning model with good generalization, i.e., with good results of predicting the unseen samples. The results obtained in this work suggest that the SVM is an effective method with great potential for classification in DCE-MRI of the breast. SVM improved the classification by producing higher A_z using each of the nine features than the discrimination power of the features alone.

LOO cross-validation has been shown to give an almost unbiased estimator of the generalization properties of statistical models, and therefore provides a sensible criterion for model selection and comparison [65]. The purpose of using model complexity controlled by the regularization parameter *C* in SVM, to constrain the optimization of empirical risk, is to avoid *overfitting*, a situation in which the decision boundary too precisely corresponds to the training data, and thereby fails on data outside the training set.

After comparing 3TP, MF-DFA 2D and MF-SELA 3D in Table III, we attribute the good performance of the proposed working scheme to the employment of the 3D and multifractal analysis in DCE-MRI of the breast. This is the main difference to the closest works with fractal theory that obtained lower classification performance (see [32], [33], [36]).

Table IV presents a comparison of the performance results from previous breast MRI CAD studies [8], [15], [17], [20], [26], [40], [41] in which A_z ranged from 0.74 to 0.97, on their private datasets. In comparison with those studies, the performance of MF-SELA with SVM feature classification appears to be in high level (0.96 with *CP*). However, the patient population differs in each study among the literature, due to the lack of a public DCE-MRI breast lesions database. Since the A_z is presumably expected to vary depending on the lesion characteristics, the A_z comparison can be regarded as less convincing. Moreover, the effects contributing to A_z variation across populations are diluted in very large databases. Despite the fact that our sample size is small, it is composed solely of cases that underwent biopsy, which

usually raise doubts in diagnosis. Therefore, we believe that it represents a good sample and the comparison of MF-SELA with the studies in Table IV is meaningful.

The developed framework raises the possibility of using measures other than lacunarity in 3D. The discriminatory potential of different 3D measures is yet to be assessed leaving an open topic to explore in the future. Moreover, it would be interesting to study the relation between multifractal parameters and tracer kinetic parameters, as kinetic texture features without having to lose the 3D information of lesions.

The proposed method could be applied to roughly any kind of tumor. A correspondence between the general anatomical structure and the possible feature-based classification of VOI is natural, by the multifractality that may prevail in medical images. The main limitation of it is to assess if the data possess multiple scaling properties or not. It is also predictable that imaging modalities with lower spatial resolution than MRI would lead to inferior discrimination power using similar scaling descriptors. In this case, the method should be calibrated with respect to the lateral size r of cubic VOI to maintain linearity in the lacunarity function. Moreover, several ranges of q should be tested for multifractal analysis to avoid unstable power laws and statistical errors.

TABLE IV
ROC A_z AMONG STATE-OF-ART STUDIES ON THEIR DATASETS

Reference	[8]	[15]	[17]	[20]	[26]	[40]	[41]
Dataset size	111	121	28	80	94	121	71
Classifier	SVM	LDA	RR	BNN	SVM	LRA	ANN
A_z	0.88	0.80	0.96	0.97	0.74	0.86	0.86

Support vector machines (SVM), linear discriminant analysis (LDA), Round-robin (RR), backpropagation neural network (BNN), linear regression analysis (LRA), artificial neural network (ANN).

VII. Conclusion

In this study, we contribute by investigating the feasibility of applying multifractal analysis using 3D lacunarity as a measure to the characterization of image texture. The VOI of the enhanced lesions revealed multiple degrees of scaling, i.e., the prevalence of a multifractal spectrum and a non linear multifractal scaling exponent. After testing the hypothesis that multifractal spectral characteristics could be related with likelihood of malignancy, our results are in line with histological ground-truth. This work suggests that the quantitative assessment of multifractal features, as proposed here, can be translated into a new and more efficient method for classification that could potentially be integrated in a computer-aided diagnosis (CADx).

References

[1] L. Moy et al., "Is breast MRI helpful in the evaluation of inconclusive mammographic findings?," *American Journal of Roentgenology*, vol. 193, no. 4, p. 986, Oct. 2009.

[2] E. Warner et al., "Surveillance of BRCA1 and BRCA2 Mutation Carriers With Magnetic Resonance Imaging, Ultrasound, Mammography, and Clinical Breast Examination," *JAMA The Journal of the American Medical Association*, vol. 292, no. 11, pp. 1317 -1325, Sep. 2004.

[3] C. Kuhl et al., "Dynamic Breast MR Imaging: Are Signal Intensity Time Course Data Useful for Differential Diagnosis of Enhancing Lesions?1," *Radiology*, vol. 211, no. 1, pp. 101-110, Apr. 1999.

[4] E. A. Morris, "Illustrated breast MR lexicon," *Seminars in Roentgenology*, vol. 36, no. 3, pp. 238-249, Jul. 2001.

[5] M. D. Schnall et al., "Diagnostic Architectural and Dynamic Features at Breast MR Imaging: Multicenter Study1," *Radiology*, vol. 238, no. 1, pp. 42 -53, Jan. 2006.

[6] B. Erguvan-Dogan, G. Whitman, A. Kushwaha, M. Phelps, and P. Dempsey, "BI-RADS-MRI: A Primer," *American Journal of Roentgenology*, vol. 187, no. 2, p. W152, Aug. 2006.

[7] S. A. Jansen et al., "DCEMRI of breast lesions: Is kinetic analysis equally effective for both mass and nonmass-like enhancement?," *Medical Physics*, vol. 35, no. 7, pp. 3102-3109, Jul. 2008.

[8] S. H. Lee et al., "Multilevel analysis of spatiotemporal association features for differentiation of tumor enhancement patterns in breast DCE-MRI," *Medical Physics*, vol. 37, no. 8, pp. 3940-3956, Aug. 2010.

[9] U. Fischer, L. Kopka, and E. Grabbe, "Breast Carcinoma: Effect of Preoperative Contrast-enhanced MR Imaging on the Therapeutic Approach1," *Radiology*, vol. 213, no. 3, pp. 881 -888, Dec. 1999.

[10] D. R. Fischer et al., "Is the 'blooming sign' a promising additional tool to determine malignancy in MR mammography?," *European Radiology*, vol. 14, no. 3, pp. 394-401, Mar. 2004.

[11] K. Kinkel and N. Hylton, "Challenges to interpretation of breast MRI," *Journal of Magnetic Resonance Imaging*, vol. 13, no. 6, pp. 821-829, Jun. 2001.

[12] Y. Gal, A. Mehnert, A. Bradley, D. Kennedy, and S. Crozier, "Feature and Classifier Selection for Automatic Classification of Lesions in Dynamic Contrast-Enhanced MRI of the breast," in *Proceedings of the 2009 Digital Image Computing: Techniques and Applications*, 2009, pp. 132-139.

[13] M. Giger, "Computerized analysis of images in the detection and diagnosis of breast cancer," *Seminars in Ultrasound CT and MRI*, vol. 25, no. 5, pp. 411-418, Oct. 2004.

[14] E. Furman-Haran, D. Grobgeld, R. Margalit, and H. Degani, "Response of MCF7 human breast cancer to tamoxifen: evaluation by the three-time-point, contrast-enhanced magnetic resonance imaging method.," *Clinical Cancer Research*, vol. 4, no. 10, pp. 2299 -2304, Oct. 1998.

[15] W. Chen, M. Giger, L. Lan, and U. Bick, "Computerized interpretation of breast MRI: Investigation of enhancement-variance dynamics," *Medical Physics*, vol. 31, no. 5, p. 1076, Apr. 2004.

[16] W. Chen, M. L. Giger, U. Bick, and G. M. Newstead, "Automatic identification and classification of characteristic kinetic curves of breast lesions on DCE-MRI," *Medical Physics*, vol. 33, no. 8, pp. 2878-2887, Aug. 2006.

[17] K. G. Gilhuijs, M. L. Giger, and U. Bick, "Computerized analysis of breast lesions in three dimensions using dynamic magnetic-resonance imaging," *Medical Physics*, vol. 25, no. 9, pp. 1647-1654, Sep. 1998.

[18] J. Yao, J. Chen, and C. Chow, "Breast Tumor Analysis in Dynamic Contrast Enhanced MRI Using Texture Features and Wavelet Transform," *IEEE Journal of Selected Topics in Signal Processing*, vol. 3, no. 1, pp. 94-100, Feb. 2009.

[19] Y. Zheng et al., "STEP: Spatiotemporal enhancement pattern for MR-based breast tumor diagnosis," *Medical physics*, vol. 36, no. 7, pp. 3192-3204, Jul. 2009.

[20] L. A. Meinel, A. H. Stolpen, K. S. Berbaum, L. L. Fajardo, and J. M. Reinhardt, "Breast MRI lesion classification: improved performance of human readers with a backpropagation neural network computer-aided diagnosis (CAD) system," *Journal of Magnetic Resonance Imaging: JMRI*, vol. 25, no. 1, pp. 89-95, Jan. 2007.

[21] T. W. Nattkemper et al., "Evaluation of radiological features for breast tumour classification in clinical screening with machine learning methods," *Artificial Intelligence in Medicine*, vol. 34, no. 2, pp. 129-139, Jun. 2005.

[22] J. Baker, P. Kornguth, J. Lo, M. Williford, and C. Floyd, "Breast cancer: prediction with artificial neural network based on BI-RADS standardized lexicon.," *Radiology*, vol. 196, no. 3, pp. 817-822, Sep. 1995.

[23] C. McLaren, W. Chen, K. Nie, and M. Su, "Prediction of Malignant Breast Lesions from MRI Features: A Comparison of Artificial Neural Network and Logistic Regression Techniques," *Academic radiology*, vol. 16, no. 7, pp. 842-851, Jul. 2009.

[24] R. Lucht, M. Knopp, and G. Brix, "Classification of signal-time curves from dynamic MR mammography by neural networks* 1," *Magnetic Resonance Imaging*, vol. 19, no. 1, pp. 51-57, Jan. 2001.

[25] T. Twellmann, O. Lichte, and T. W. Nattkemper, "An adaptive tissue characterization network for model-free visualization of dynamic contrast-enhanced magnetic resonance image data," *IEEE Trans. Med. Imaging*, vol. 24, no. 10, pp. 1256-1266, Oct. 2005.

[26] J. Levman, T. Leung, P. Causer, D. Plewes, and A. L. Martel, "Classification of Dynamic Contrast-Enhanced Magnetic Resonance Breast Lesions by Support Vector Machines," *IEEE Trans. Med. Imaging*, vol. 27, no. 5, pp. 688-696, May. 2008.

[27] A. Basavanhally, S. Doyle, and A. Madabhushi, "Predicting classifier performance with a small training set: Applications to computer-aided diagnosis and prognosis," in *Proceedings of the IEEE International Symposium on Biomedical Imaging: From Nano to Macro*, 2010, pp. 229-232.

[28] D. Newell et al., "Selection of diagnostic features on breast MRI to differentiate between malignant and benign lesions using computer-aided diagnosis: differences in lesions presenting as mass and non-mass-like enhancement," *European Radiology*, vol. 20, no. 4, pp. 771-781, Apr. 2010.

[29] P. Hayton, M. Brady, L. Tarassenko, and N. Moore, "Analysis of dynamic MR breast images using a model of contrast enhancement," *Medical Image Analysis*, vol. 1, no. 3, pp. 207-224, Apr. 1997.

[30] L. Arbach, A. Stolpen, and J. Reinhardt, "Classification of breast MRI lesions using a backpropagation neural network (BNN)," in *Proceedings of the IEEE International Symposium on Biomedical Imaging: Nano to Macro*, 2004, pp. 253-256.

[31] Q. Wu and M. Markey, "Computer-Aided Diagnosis of Breast Cancer on MR Imaging," in *Recent Advances in Breast Imaging, Mammography, and Computer-Aided Diagnosis of Breast Cancer*, vol. 1555, SPIE Press, 2006, pp. 743-766.

[32] A. Penn et al., "Morphologic Blooming in Breast MRI as a Characterization of Margin for Discriminating Benign from Malignant Lesions," *Academic radiology*, vol. 13, no. 11, pp. 1344-1354, Nov. 2006.

[33] A. I. Penn, L. Bolinger, M. D. Schnall, and M. H. Loew, "Discrimination of MR images of breast masses with fractal-interpolation function models," *Academic Radiology*, vol. 6, no. 3, pp. 156-163, Mar. 1999.

[34] F. Soares, M. M. Freire, M. Pereira, F. Janela, and J. Seabra, "Towards the detection of microcalcifications on mammograms through Multifractal Detrended Fluctuation Analysis," in *Proceedings of the IEEE Pacific Rim Conference on Communications, Computers and Signal Processing*, 2009, pp. 677-681.

[35] F. Soares, F. Janela, J. Seabra, M. Pereira, and M. M. Freire, "Self-similarity classification of breast tumour lesions on dynamic contrast-enhanced magnetic resonance images - Special Session on Breast CAD," *International Journal of Computer Assisted Radiology and Surgery*, vol. 5, no. 1, pp. S203-S205, Jun. 2010.

[36] A. Penn, S. Thompson, M. Schnall, M. Loew, and L. Bolinger, "Fractal discrimination of MRI breast masses using multiple segmentations," in *Proceedings of SPIE*, 2000, vol. 3979, pp. 959-966.

[37] H. O. Peitgen, H. Jürgens, and D. Saupe, *Chaos and Fractals: New Frontiers of Sciences*. Springer, 1993.

[38] Q. Guo, J. Shao, and V. Ruiz, "Characterization and classification of tumor lesions using computerized fractal-based texture analysis and support vector machines in digital mammograms," *International Journal of Computer Assisted Radiology and Surgery*, vol. 4, no. 1, pp. 11-25, 2009.

[39] R. Lopes, P. Dubois, I. Bhouri, M. Bedoui, S. Maouche, and N. Betrouni, "Local fractal and multifractal features for volumic texture characterization," *Pattern Recognition*, vol. 44, no. 8, pp. 1690-1697, 2011.

[40] W. Chen, M. L. Giger, H. Li, U. Bick, and G. M. Newstead, "Volumetric texture analysis of breast lesions on contrast-enhanced magnetic resonance images," *Magnetic Resonance in Medicine*, vol. 58, no. 3, pp. 562-571, 2007.

[41] K. Nie, J.-H. Chen, H. J. Yu, Y. Chu, O. Nalcioglu, and M.-Y. Su, "Quantitative Analysis of Lesion Morphology and Texture Features for Diagnostic Prediction in Breast MRI," *Academic radiology*, vol. 15, no. 12, pp. 1513-1525, Dec. 2008.

[42] R. Lopes and N. Betrouni, "Fractal and multifractal analysis: A review," *Medical Image Analysis*, vol. 13, no. 4, pp. 634-649, Aug. 2009.

[43] C. J. Rose et al., "Quantifying spatial heterogeneity in dynamic contrast-enhanced MRI parameter maps," *Magnetic Resonance in Medicine*, vol. 62, no. 2, pp. 488-499, 2009.

[44] R. Riedi, "Multifractal processes," in *Theory and Applications of Long Range Dependence*, P. Doukhan, G. Oppenheim, and MS Taqqu, eds., Birkhäuser, Boston, 2003, pp. 625-716.

[45] Q. Cheng, "Multifractal modeling and lacunarity analysis," *Mathematical Geology*, vol. 29, no. 7, pp. 919-932, 1997.

[46] P. Ciuciu, P. Abry, C. Rabrait, and H. Wendt, "Log Wavelet Leaders Cumulant Based Multifractal Analysis of EVI fMRI Time Series: Evidence of Scaling in Ongoing and Evoked Brain Activity," *IEEE Journal of Selected Topics in Signal Processing*, vol. 2, no. 6, pp. 929-943, 2008.

[47] C. Tolle, T. Mcjunkin, and D. Gorsich, "An efficient implementation of the gliding box lacunarity algorithm," *Physica D: Nonlinear Phenomena*, vol. 237, no. 3, pp. 306-315, 2008.

[48] P. Dong, "Lacunarity analysis of raster datasets and 1D, 2D, and 3D point patterns," *Computers & Geosciences*, vol. 35, no. 10, pp. 2100-2110, 2009.

[49] G. Dougherty and G. M. Henebry, "Lacunarity analysis of spatial pattern in CT images of vertebral trabecular bone for assessing osteoporosis," *Medical engineering & physics*, vol. 24, no. 2, pp. 129-138, 2002.

[50] C. Allain and M. Cloitre, "Characterizing the lacunarity of random and deterministic fractal sets," *Physical review A*, vol. 44, no. 6, p. 3552, 1991.

[51] R. E. Plotnick, R. H. Gardner, W. W. Hargrove, K. Prestegaard, and M. Perlmutter, "Lacunarity analysis: A general technique for the analysis of spatial patterns," *Physical Review E*, vol. 53, no. 5, p. 5461, May. 1996.

[52] S. W. Myint and N. Lam, "A study of lacunarity-based texture analysis approaches to improve urban image classification," *Computers, Environment and Urban Systems*, vol. 29, no. 5, pp. 501-523, Sep. 2005.

[53] S. Stach, J. Cybo, J. Cwajna, and S. Roskosz, "Multifractal description of fracture morphology. Full 3D analysis of a fracture surface," *Materials Science-Poland*, vol. 23, no. 2, 2005.

[54] P. Dong, "Test of a new lacunarity estimation method for image texture analysis," *International Journal of Remote Sensing*, vol. 21, no. 17, pp. 3369-3373, 2000.

[55] A. Hanen, B. Imen, B. A. Asma, D. Patrick, and B. M. Hédi, "Multifractal modelling and 3D lacunarity analysis," *Physics Letters A*, vol. 373, no. 40, pp. 3604-3609, 2009.

[56] D. Fabio, A. Reis, and R. Riera, "Lacunarity calculation in the true fractal limit," *Journal of Physics A: Mathematical and General*, vol. 27, p. 1827, 1994.

[57] M. Domon and E. Honda, "Correlation of measured fractal dimensions with lacunarities in computer-generated three-dimensional images of Cantor sets and those of fractional Brownian motion," *FORMA-TOKYO-*, vol. 14, no. 3, pp. 249-263, 1999.

[58] L. Zhang, J. Z. Liu, D. Dean, V. Sahgal, and G. H. Yue, "A three-dimensional fractal analysis method for quantifying white matter structure in human brain," *Journal of neuroscience methods*, vol. 150, no. 2, pp. 242-253, 2006.

[59] Q. Cheng, "The gliding box method for multifractal modeling," *Computers & geosciences*, vol. 25, no. 9, pp. 1073-1079, 1999.

[60] Y. Shimizu, M. Barth, C. Windischberger, E. Moser, and S. Thurner, "Wavelet-based multifractal analysis of fMRI time series," *NeuroImage*, vol. 22, no. 3, pp. 1195-1202, Jul. 2004.

[61] J. Delour, J. F. Muzy, and A. Arnéodo, "Intermittency of 1D velocity spatial profiles in turbulence: a magnitude cumulant analysis," *The European Physical Journal B*, vol. 23, no. 2, pp. 243-248, 2001.

[62] H. Wendt, P. Abry, and S. Jaffard, "Bootstrap for empirical multifractal analysis," *IEEE Signal Processing Magazine*, vol. 24, no. 4, pp. 38-48, 2007.

[63] B. Szabo, P. Aspelin, M. Kristoffersen Wiberg, and B. Bone, "Dynamic MR imaging of the breast: analysis of kinetic and morphologic diagnostic criteria," *Acta Radiologica*, vol. 44, no. 4, pp. 379-386, Jul. 2003.

[64] T. Joachims, *Making large-scale SVM learning practical*. MIT press, 1999.

[65] J. Ramana and D. Gupta, "LipocalinPred: a SVM-based method for prediction of lipocalins," *BMC bioinformatics*, vol. 10, no. 1, p. 445, 2009.

[66] K. H. Brodersen, C. S. Ong, K. E. Stephan, and J. M. Buhmann, "The binormal assumption on precision-recall curves," presented at the Pattern Recognition (ICPR), 2010 20th International Conference on, 2010, pp. 4263-4266.

Filipe Soares is a computer scientist specialized in the field of medical image processing and decision support systems. He received the 5-year B.Sc. degree in Computer Science and Engineering in 2006 from University of Beira Interior (UBI), Portugal. He has been working as a researcher at Siemens S.A. Healthcare Sector, Portugal. He is a Ph.D. Student in Computer Science and Engineering from UBI, focused on computer-aided diagnosis (CAD) in breast cancer. His work led to the development of prototype software with innovative detection of microcalcifications in Mammography and breast masses in Magnetic Resonance Imaging, for which he received the Siemens Innovation Award in 2012. He is the author or co-author of 8 papers in refereed international journals and conferences, and the author of a chapter in book. His main research interests include: software engineering, image processing, breast cancer, multifractal and wavelet analysis, computer-aided diagnosis, pattern recognition, artificial intelligence, computer networks and bioinformatics.

Filipe Janela received the 5-year B.Sc. degree in Chemical Engineering in 2004, and post-graduation in Engineering and Technology Management in 2007, both from Instituto Superior Técnico of the Technical University of Lisbon, Portugal. In 2012, he concluded a Master in Business Administration (MBA) from IESE/AESE School of Management. His career started in 2004, as a process engineer in the Oil & Energy Sector at Norsk Hydro, Norway. In the following years he engaged the business consulting, integrating Siemens S.A. Healthcare Sector in 2006. He is currently the Head of Innovation and Collaboration and owner of Innovation Program of Siemens Healthcare Sector, Portugal. He is the co-author of several papers in refereed international journals and conferences. During his career he developed competences in the fields of strategic consulting, business development management, technology and innovation management, research and development.

Manuela Pereira received the 5-year B.Sc. degree in Mathematics and Computer Science in 1994 and the M.Sc. degree in Computational Mathematics in 1999, both from the University of Minho, Portugal. She received the Ph.D. degree in Signal and Image Processing in 2004 from the University of Nice Sophia Antipolis, France. She is an Assistant Professor of Computer Science at the University of Beira Interior, Portugal. Her main research interests include: multiple description coding, joint source/channel coding, image and video coding, holographic 3D video coding, wavelet analysis, information theory, image segmentation and real-time video streaming, Quality of Experience (QoE) assessment and QoE modeling. She is the co-editor of 6 books and has authored or co-authored around 50 papers in international refereed journals and conferences. She served as a technical and program committee member for several IEEE journals and conferences. She is also a member of the editorial review board of several international journals.

João Seabra received the 5-year B.Sc. degree in Electric and Computer Engineering in 1997, from Faculty of Engineering of the University of Porto, Portugal. He started his professional activity at Siemens, in the operating group Medical Solutions. He is currently the General Manager of Siemens Healthcare Sector in Portugal, and Division Cluster Lead for the region of Southwest Europe. During his career he developed competences in the fields of imaging systems and healthcare IT, playing roles in the areas of project management, product and business management. He is member of Siemens Corporate Executive Committee in Portugal, where he is responsible for the corporate areas of Innovation and Globalization. Besides his duties at Siemens, he also played administration roles in Amb3E (Electrical and Electronic Waste Management Company) and AEP (Portuguese Enterprise Association). From 2010 to 2012, he was member of the General Counsel in University of Beira Interior, Portugal.

Mário M. Freire received the 5-year B.Sc. degree in Electrical Engineering and the 3-year M.Sc. degree in Systems and Automation in 1992 and 1994, respectively, from the University of Coimbra, Portugal. He received the Ph.D. degree in Electrical Engineering in 2000 and the Habilitation title in Computer Science in 2007 from the University of Beira Interior, Portugal. He is a full professor of Computer Science at University of Beira Interior, which he joined in the fall of 1994. When he was a M.Sc. student at University of Coimbra, he was also a trainee researcher for a short period in 1993 in the Research Centre of Alcatel-SEL (now Alcatel-Lucent) in Stuttgart, Germany. His main research interests include multimedia networking and peer-to-peer systems, multimedia traffic analysis and synthesis, network forensics and security, and data centers and cloud computing. He is the co-author of seven international patents, co-editor of eight books published in the Springer Lecture Notes in Computer Science book series, and author or co-author of about 120 papers in refereed international journals and conferences. He serves as a member of the editorial board of the ACM SIGAPP Applied Computing Review, serves as associate editor of the Wiley Journal on Security and Communication Networks, and served as editor of the IEEE Communications Surveys and Tutorials. He also served as a guest editor of two feature topics in IEEE Communications Magazine and of a special issue of Wiley International Journal of Communication Systems. He served as a technical program committee member for several IEEE international conferences and is co-chair of the Track on Networking of the ACM SAC 2014. He is a chartered engineer by the Portuguese Order of Engineers and he is member of the IEEE Computer Society and the IEEE Communications Society, and member of the Association for Computing Machinery.